ADVANCED MATERIALS

www.advmat.de

Optothermally Programmable Liquids with Spatiotemporal Precision and Functional Complexity

Xixi Chen, Tianli Wu, Danmin Huang, Jiajia Zhou, Fengxiang Zhou, Mei Tu, Yao Zhang, Baojun Li, Yuchao Li, and Lingxiang Jiang**

Due to the intrinsic lack of spatial order and self-supported shape, liquids are often incompatible with precision manufacturing/processing and are potentially limited for advanced functionality. Herein, an optothermal strategy is developed to fully command phase-separated liquids with unprecedented spatiotemporal addressability. Specifically, a laser is focused onto an Au film to create a hot spot that locally demixes a temperature-responsive solution to produce a single optothermal droplet. Spatial precision is assured by the well-defined thermal field and temporal accuracy guaranteed by the fast heating and response rate. Time-multiplexed laser foci are deployed to engineer the thermal landscape as desired, which in turn dictates the formation/dissolution, positioning, shaping, and dynamic reconfiguration of the phase-separated liquids. Further, laser foci are programmed to orchestrate the liquid patterns in a time-continuous manner to produce liquid animations on the microscale with high fidelity. While focused lasers are routinely used to manipulate solid particles or to microfabricate solid materials, the current strategy embraces the merits of liquids and features functional complexity in information encryption, payload transportation, and reaction localization. The strategy is further applicable in scenarios such as subcellular organization of biomolecular condensates and programmable modulation of non-equilibrium systems.

1. Introduction

An ongoing endeavor in chemistry and materials science is to construct reconfigurable matter and to manipulate them with spatiotemporal precision and functional complexity.[1] Central to this endeavor are two nontrivial tasks—how to encode desired responsiveness into target materials and how to trigger their responses in an efficient, accurate, and programmable manner? The answers are particularly elusive for liquids[2,3] that are inherently disordered and shapeless because the current wisdom is largely limited to (partially) ordered materials by dynamically reconfiguring, for example, lattices of crystals,[4] molecular alignments of liquid crystals,[5] and mesh sizes of polymer networks.[6]

Living cells, in great contrast, have mastered a set of sophisticated strategies to regulate liquid assemblies such as membraneless organelles to spatiotemporally organize subcellular contents in response to environmental cues or biological cycles for physiological functionality.[7] Liquid–liquid phase separation (LLPS) was recognized as the key mechanism to drive the formation of such liquid condensates, yet its stochastic nature (especially susceptible to thermal fluctuations) poses a grand challenge for its precise control.[8,9] Cells counter this randomness to some extent by virtue of morphogen gradients or post-translational modifications.[10] In the synthetic realm, researchers attempted to modulate phase-separated liquids via acoustic waves,[11] electrical fields,[12] and light irradiation.[9,13] The current in vivo or in vitro means, however, cannot impose a tight spatial control or attain a fast temporal response.[14]

Herein, we report on an optothermal strategy to dynamically control phase-separated liquids with an unprecedented level of spatiotemporal addressability and a rich variety of functions (**Figure 1**). First, we identify representative LLPS systems (biotic or otherwise) that demix upon heating beyond a critical temperature (T_c) to produce condensed droplets in equilibrium with a dilute phase (Figure 1a).[15,16] Second, we apply a tightly focused laser onto a gold film to create a hot spot with temperature radially decaying outward, producing a single phase-separated droplet confined inside a critical dome (referred to as

X. Chen, T. Wu, Y. Zhang, B. Li, Y. Li
Institute of Nanophotonics
Jinan University
Guangzhou 511443, China
E-mail: liyuchao@jnu.edu.cn

D. Huang, M. Tu
College of Chemistry and Materials Science
Jinan University
Guangzhou 510632, China

D. Huang, J. Zhou, F. Zhou, L. Jiang
South China Advanced Institute for Soft Matter Science and Technology
School of Emergent Soft Matter
South China University of Technology
Guangzhou 510640, China
E-mail: jianglx@scut.edu.cn

J. Zhou, F. Zhou, L. Jiang
Guangdong Provincial Key Laboratory of Functional and Intelligent Hybrid Materials and Devices
South China University of Technology
Guangzhou 510640, China

The ORCID identification number(s) for the author(s) of this article can be found under https://doi.org/10.1002/adma.202205563.

DOI: 10.1002/adma.202205563

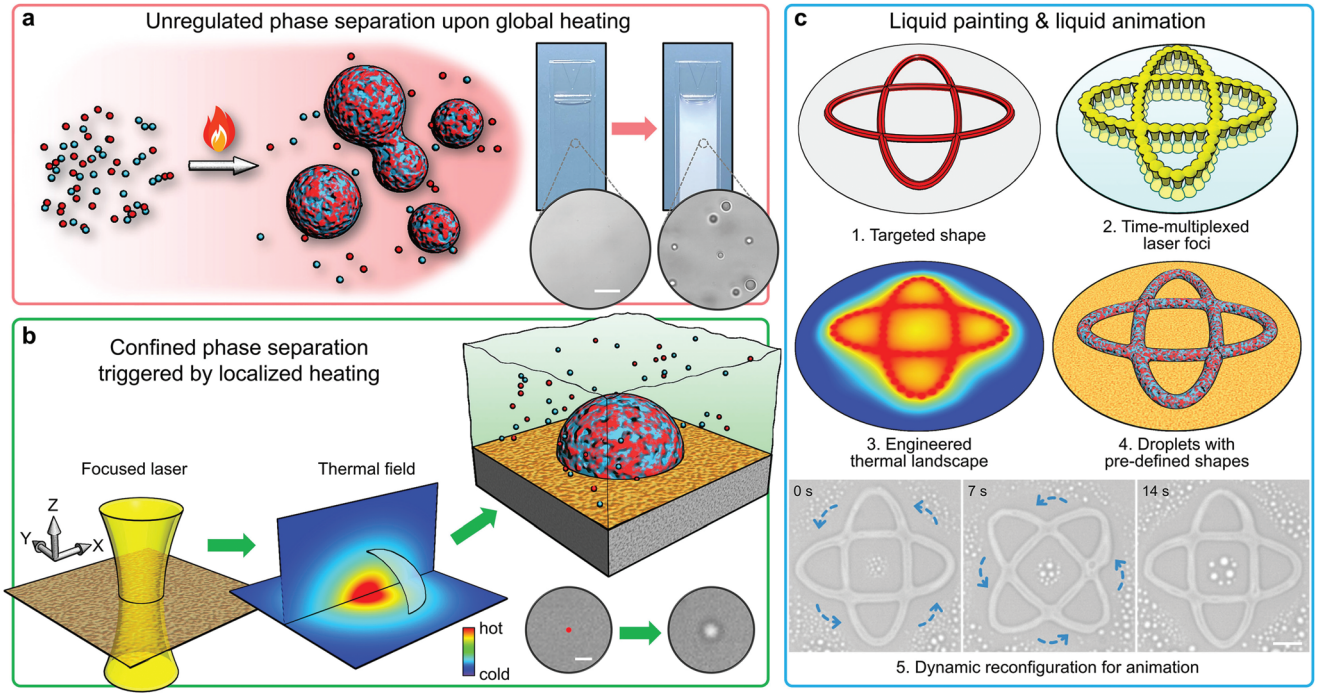

Figure 1. Schematic representation of the optothermally programable liquids. a) An aqueous mixture of two molecules (red and cyan) undergoes liquid–liquid phase separation upon heating. Global heating, however, produces massive droplets randomly distributed in the cuvette. b) Focusing a laser on an Au film can efficiently convert photons to heat that creates a localized dome, under which the solution is superheated for condensation. c) A simplified guide to program the optothermal liquids by carving the thermal landscape. Generation of a liquid painting to recapitulate a target shape (c1–c4) and dynamical reconfiguration of the painting toward animation (c5). Scale bars = 10 µm (a), 2 µm (b), and 5 µm (c). Demonstrative experiments are performed on Sys. 1.

optothermal droplet, Figure 1b). Third, time-multiplexed laser foci are employed to precisely define the thermal landscape on demand such that we can command the droplets in a manifold manner, including their formation/dissolution, position, shape/size, and dynamic behavior; in doing so, we realize liquid painting and liquid animation with high fidelity (Figure 1c; Movie S1, Supporting Information). Finally, we demonstrate applications of the programmable liquids in information encryption, payload transportation, and reaction localization.

2. Results and Discussion

In a typical experiment, an aliquot of Sys. 1 solution is sandwiched between an Au-coated glass slide and a coverslip (see Note S1, Supporting Information for the optical setup). Sys. 1 refers to aqueous solutions of DTAB (dodecyltrimethylammonium bromid) and PTS (pyrenetetrasulfonate tetrasodium), which undergo acute phase separation (coacervation) upon heating (see Notes S2 and S3, Supporting Information for more information on thermally responsive LLPS systems). Its critical temperature T_c strongly depends on composition (Figure S6, Supporting Information), and we mainly present optothermal results on composition A (DTAB/PTS = 20/10 $\times 10^{-3}$ M) with T_c = 41 °C in the vicinity of body temperature and composition B (DTAB/PTS = 60/30 $\times 10^{-3}$ M) with T_c = 55 °C. The sample is mounted onto a microscope stage, in which a low-power laser (3–10 mW, 1064 nm) is focused onto the Au film with a beam radius of 0.7 µm. The irradiated spot effectively turns incident light into heat and quickly establishes a stable thermal field in ≈20 ms,[17] where spatially dependent temperature is elevated to ≈57 °C at the hot spot and hyperbolically decays outward (**Figure 2**a; Note S4, Supporting Information Sys. 1 and T_c = 41 °C). In this radial thermal field, we define a dome-shaped isothermal surface of T_c as the critical dome, under which the solution is superheated for phase separation and outside of which underheated. Real-time inspection on the kinetics of droplet formation reveals three distinct periods (Figure 2b,c; Movie S2, Supporting Information). In the induction stage, droplet nucleation is triggered at the hot spot followed by initial growth (yet too small to resolve optically). In the growth stage, droplet radius (r_{drop}) increases at a rate proportional to $t^{1/3}$, in line with the characteristic scaling law of a diffusion-controlled Lifshitz-Slyozov process.[18] In the last stage, the droplet is in a steady state except for slow expansion due to heat accumulation in the chamber.

To qualitatively recapitulate this localized phase separation, we construct a minimum, Flory–Huggins model for a binary system with the interaction parameter χ related to temperature (Figure 2d; Note S5, Supporting Information). Given a hyperbolic temperature profile, phase separation indeed occurs with the condensed phase confined to the hot region. Notably the phase boundary aligns with the position of T_c, indicating that condensation is limited within the critical dome such that $r_{drop} \approx r_{dome}$. This conformity of phase separation to the thermal landscape is crucial to the fidelity of liquid painting and

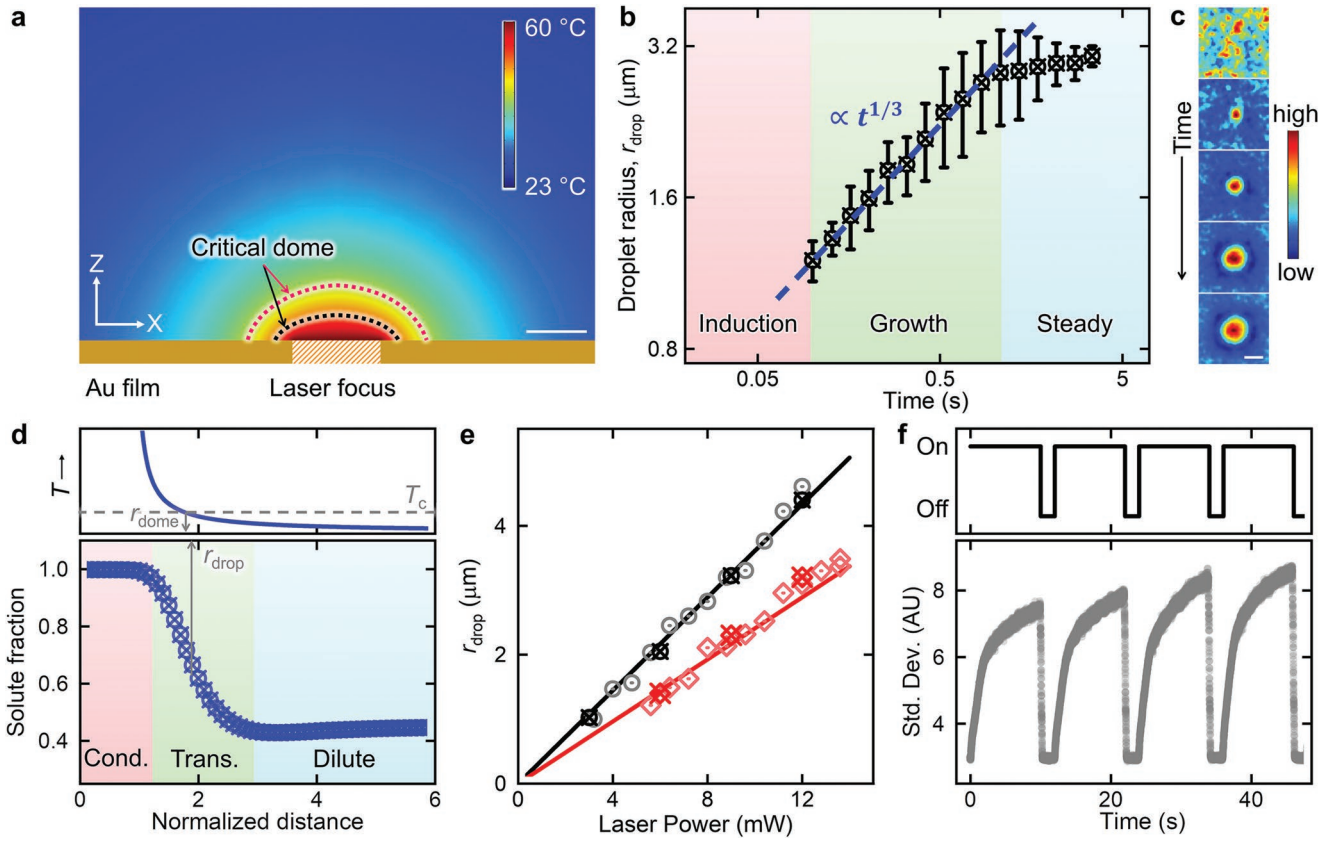

Figure 2. Kinetics and thermodynamics of droplet formation and dissolution upon laser irradiation and removal, respectively. a) Simulated temperature profile around the laser focus in the *XZ* plane (Note S4, Supporting Information). Critical domes corresponding to T_c = 41 and 55 °C are highlighted by red and black dash lines, respectively. b) Droplet radius r_{drop} as a function of time upon laser irradiation, where three distinctive stages are color coded. c) Appearance and growth of an optothermal droplet. The grayscale, bright-field images are converted into heat maps (rainbow color coded) for better visualization. d) Phase separation in a temperature gradient as simulated by a minimal Flory–Huggins model (Note S5, Supporting Information). The system is in condensed, transition, and dilute states as dictated by local temperature (notably, $r_{drop} \approx r_{dome}$). e) Linear dependence of r_{drop} on laser power for T_c = 41 and 55 °C samples (red and black, composition A and B) as confirmed by experiments (dark dots), simulations (pale dots), and theory (lines, Note S5, Supporting Information). f) Repetitive laser on/off triggers droplet formation/dissolution for at least 15 cycles (not shown in full). Standard deviation of an image can reflect droplet size and its computation is more straightforward and reliable than tracking size directly.[22] Scale bars = 1 μm (a) and 3 μm (c). Experiments are performed on Sys. 1.

animation as we will show later. We then precisely control r_{drop} by adjusting laser power, for which a linear dependence is corroborated by experimental, theoretical, and simulation results (Figure 2e; Note S5.3, Supporting Information). Removal of laser swiftly causes droplet shrinkage and dissolution; consecutive on/off circles lead to repetitive droplet formation/dissolution without hysteresis (Figure 2f; Movie S3, Supporting Information). A gradual, upward shifting is observed with repeated circles (Figure 2f, lower panel), relevant to the previously speculated heat accumulation (the steady stage in Figure 2b). We perform a control experiment by waiting 5 min (laser off) between circles for the chamber to dissipate all the extra heat. In this case, the curves of standard deviation are identical (data not shown), thus supporting our speculation. Similar optothermal experimental results on Sys. 2 to 7 affirm generality of this optothermal strategy for LLPS systems with a lower critical solution temperature (LCST, Note S2.2, Supporting Information).

It is generally difficult to optically deform a solid particle or liquid droplet because the radiation force of a continuous-wave laser is feeble in comparison to the Young's modulus of the former or surface tension (σ) of the latter.[19] The current strategy, in contrast, allows us to sculpture the optothermal liquids (usually of low $\sigma < 1$ mN m^{-1}) into virtually arbitrary shapes by engineering the thermal landscape. Practically, we arrange laser foci in different patterns, verify the geometry of critical domes by simulation, and obtain droplets of designed shapes experimentally. Representatively, the optothermal droplets are shaped into a line, a ring, a triangle, and a square (**Figure 3**a–e, Sys. 1). As a rule of thumb, the shape resolution is ≈0.75 μm (linewidth and radius of curvature respectively highlighted in Figure 3b,e), likely determined by the beam radius; it is thus possible to improve the resolution by reducing the beam size. We can also generate an 8 × 8 array of discrete droplets with a positional accuracy ≈30 nm by deploying regularly spaced laser foci (Figure 3f; Movie S4, Supporting Information), in which each droplet can be, in principle, further manipulated independently. We then create liquid paintings of complexity by replicating two panda sketches, in which high fidelity is achieved by proper segmentation of curves and tessellation of

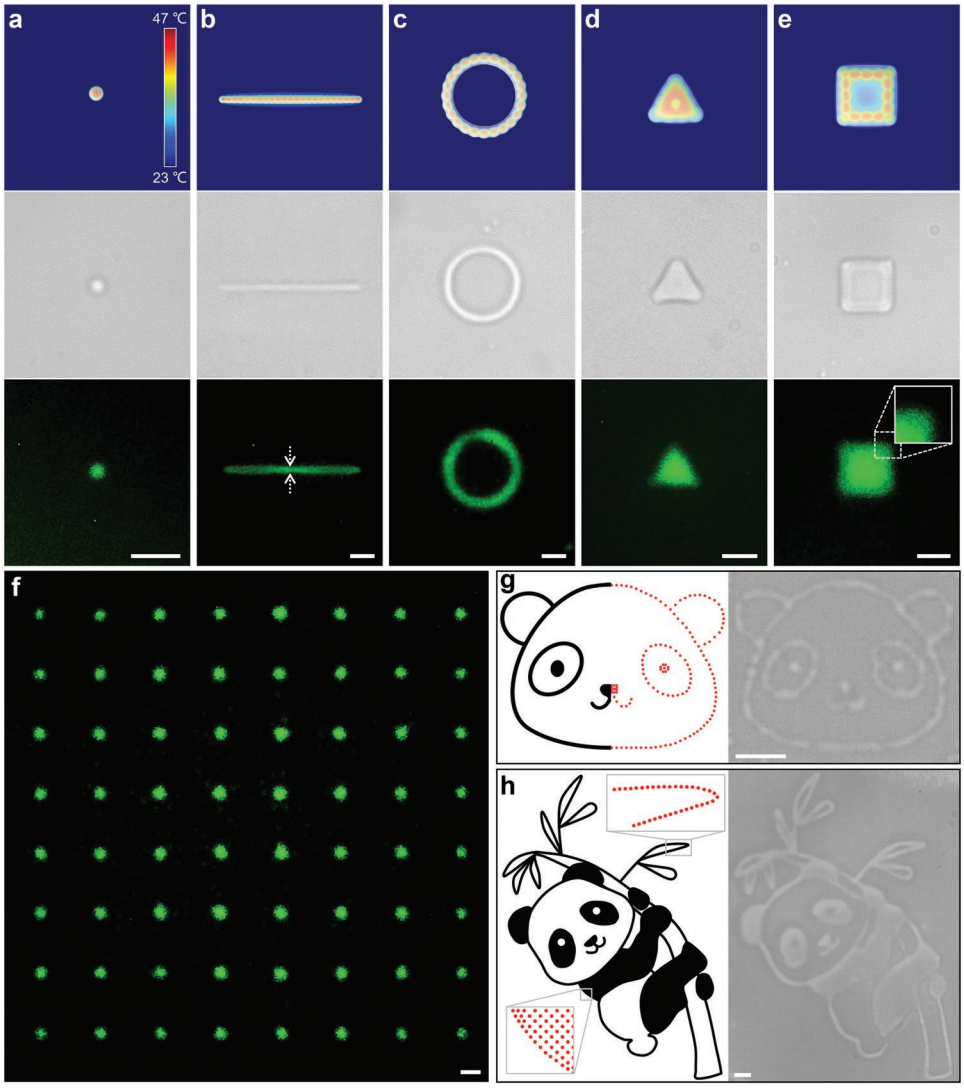

Figure 3. Liquid painting by optothermal phase separation. a–e) Properly deployed laser foci can generate dot, linear, circular, triangular, and square droplets. The images from top to bottom are simulated temperature maps, bright-field pictures, and fluorescence pictures, respectively. The line width and curvature radius are highlighted in (b) and (e), respectively. f) An 8 × 8 array of discrete droplets. g,h) Two panda sketches are recapitulated by optothermal liquid painting with high fidelity. The red dots indicate laser foci, highlighting segmentation of curves and tessellation of areas. Scale bars = 5 µm. Experiments are performed on Sys. 1.

areas (Figure 3g,h). Once the laser is removed, these liquid paintings can quickly erase themselves and revert to a single-phase solution with no trace of any kind, suggesting potential applications in information encryption.

Next, we set to dynamically maneuver the droplets. When a laser focus is steered at a constant velocity (v_{laser}), the droplet can track it up to an escape velocity (v_{esc}) albeit stretched in the moving direction; the dislocation between the droplet center and laser focus reaches a steady value that is roughly proportional to v_{laser} and insensitive to laser power (**Figure 4**a,b; Movie S5, Supporting Information Sys. 1). When the laser motion stops, the droplet regains its original shape and recenters around the laser focus, indicating a restoring force at work (Figure 4b, $v_{laser} \approx v_{esc}$). Beyond v_{esc}, the laser focus takes a small fraction of the droplet to detach from the original one; then the original droplet dissolves while the new one grows (Figure 4b, $v_{laser} > v_{esc}$). Quantitative calculations reveal that the droplet motion is not driven by optical trapping force[20] (negligibly small due to low laser power) but by thermocapillary force[21] (thermotaxis in our case) and by droplet remodeling (Note S6, Supporting Information). In particular, the remodeling is of a nonequilibrium nature in response to heat source repositioning.[22] Influx and condensation of solutes occur preferably at the warmer front, while outflux and dissolution take place at the cooler rear; in effect, it moves the droplet toward the heat source. The droplets can follow prescribed rectilinear or curvilinear trajectories despite slight mismatch at sharp corners (Figure 4c; Movie S6, Supporting Information).

Drastically distinct from solid particles that lack reconfigurability,[23] the optothermal droplets are fluidic in nature and can thus be programed to form/dissolve (Figure 2), fuse/fission (Figure 4d; Movie S7, Supporting Information), resize, and

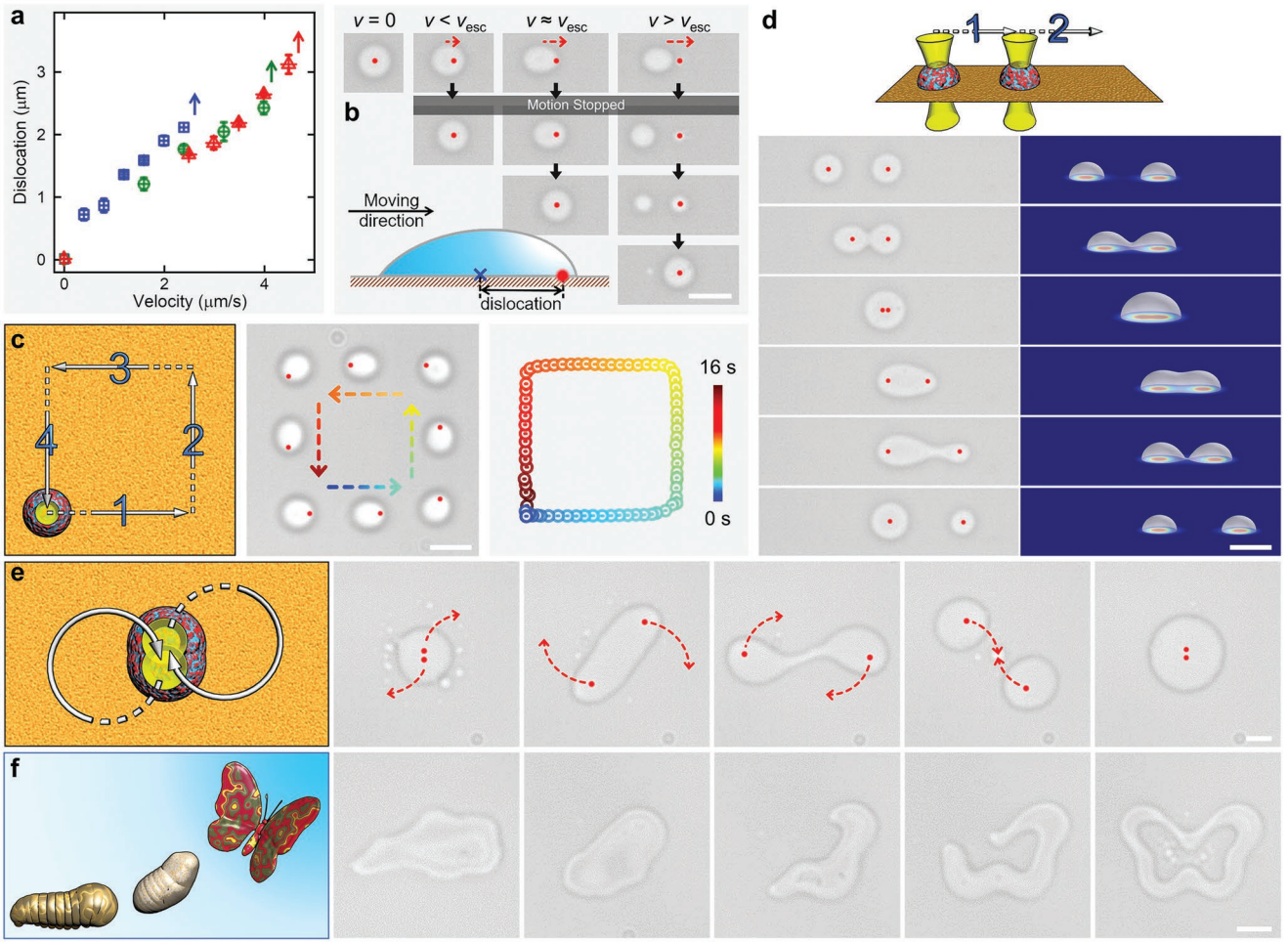

Figure 4. Animation of programmable liquids. a–c) Steering a droplet by moving the laser. Dislocation between the droplet center and laser focus as a function of laser velocity (a) at different laser powers (6, 8, and 10 mW for blue, green, and red dots, respectively). The arrows denote the escape velocity (v_{esc}). Droplet deformation when $v \leq v_{esc}$, droplet division when $v > v_{esc}$, and droplet restoration when laser motion is stopped (b, Note S6, Supporting Information). The droplet follows a rectilinear path as designed (c). d) Droplet fusion and fission. e) Droplets moving in an 8-shaped track. f) Transformation of a caterpillar to a cocoon and a butterfly. Scale bars = 5 μm. Experiments are performed on Sys. 1.

reshape. We thus create liquid animation on the microscale by performing successive, complex operations on multiple droplets in a fashion conceptually akin to filmmaking. Representative animations include a rotating orbit (Figure 1c; Movie S1, Supporting Information), number counting (Movie S8, Supporting Information), two droplets moving in an 8-shaped track (Figure 4d; Movie S9, Supporting Information), and transformation of a caterpillar to a cocoon and a butterfly (Figure 4e; Movie S10, Supporting Information). Critical to the implementation of liquid animation is the acousto-optic deflector (AOD)-based technique that can deflect a single laser beam at a high frequency (up to 100 kHz) to generate multiple foci (up to 2500) in a 100 × 100 μm^2 working field (Note S1, Supporting Information). This time-multiplex approach further enables us to reconfigure the thermal landscape at will by independently controlling the position and power of each focus.

Provided with the remarkable spatiotemporal addressability, we explore applications of this optothermal strategy in information coding, payload transportation, and reaction localization. Music visualization is an automated process that converts an audio into a time series of frequency spectra followed by visual rendering into various representations such as dynamic bar graphs (**Figure 5**a, Sys. 1). The visualizer is miniaturized and liquidated here by replacing the bars with optothermal droplets such that their heights and lateral positions reflect sound amplitude and frequency, respectively. To this end, we input a vibrate music "Croatian Rhapsody" that accesses a wide frequency range and output a liquid animation of nine droplets hopping in rhythm (Figure 5a, Movie S11, Supporting Information). At the current stage, the animation is outpaced by the fast-tempo music due to the limited droplet response time, so it is compiled at a 70× speed to reach audio-visual synchronization.

Conventional optical tweezers face fundamental challenges in the cases of low refractive-index contrast (low-Δn, like intracellular organelles) or sub-10 nm objects when optical gradient force is overwhelmed by Brownian motion.[24] We sidestep these limitations by leveraging the optothermal phase separation and subsequent payload partitioning that is essentially independent of Δn or size.[25] Indeed, the optothermal droplets exhibit remarkable capacity to enrich and compartmentalize a

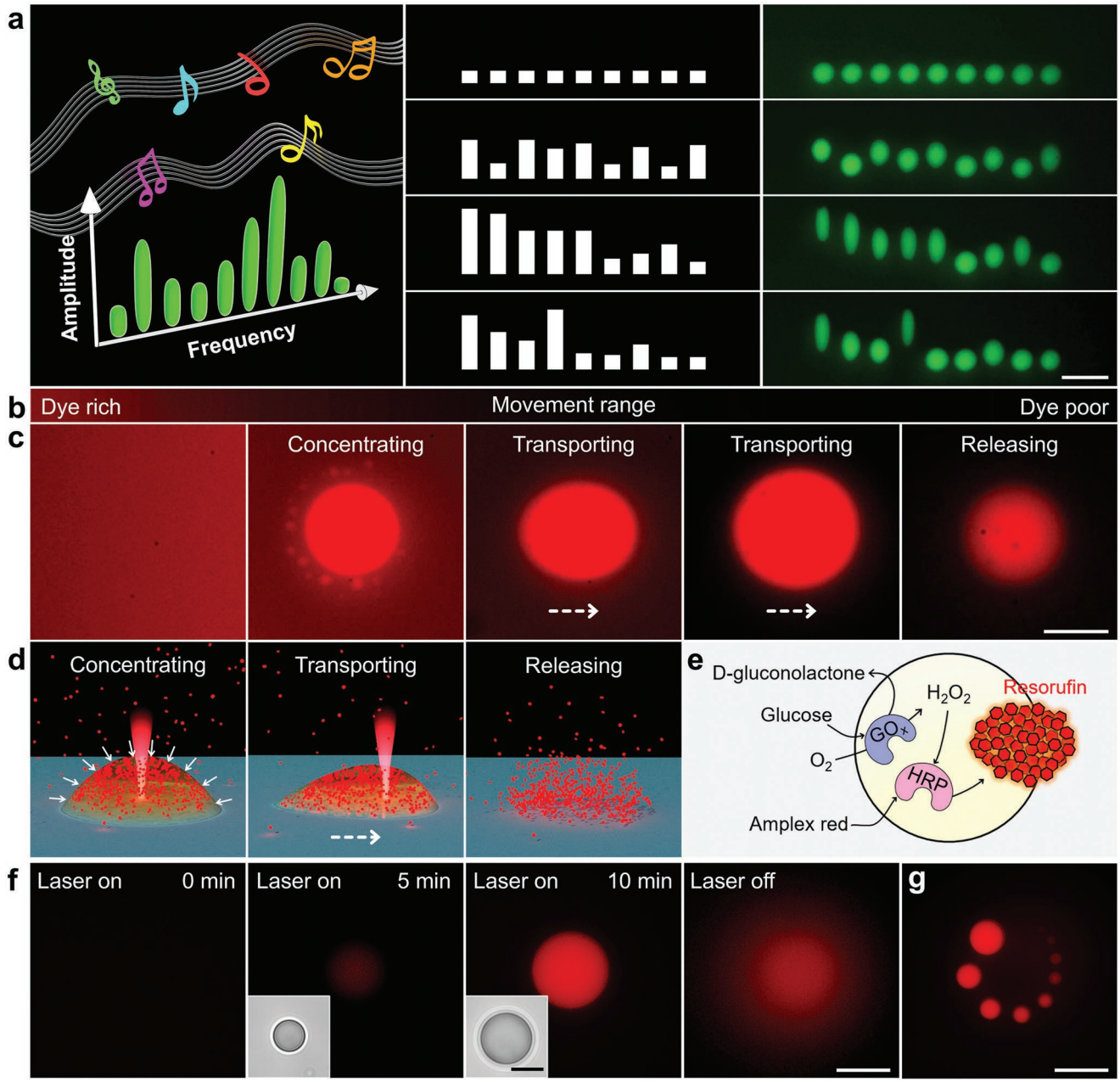

Figure 5. Applications of programmable liquids in information coding (a), cargo transportation (b–d), and microreactors (e–g). a) Liquidated music visualizer, where a music is converted to a dynamic bar graph and further to a row of droplets hopping in rhythm. Two axes represent frequency and amplitude, respectively. b–d) Enrichment, transportation, and release of a dye from a dye-rich to a dye-poor region across a range of 360 µm. e–g) An optothermal droplet acts as a microreactor (f) to host a cascade reaction catalyzed by two sequential enzymes (e). We can further control the position, size, and on/off states of each microreactor (g). Scale bars = 20 µm (a,f,g) and 10 µm (c). Experiments are performed on Sys. 1 (a–c) and on Sys. 2 (f,g).

variety of guests, including small molecules (<1 nm), proteins, and nano- or microparticles (Note S7, Supporting Information), many of which are difficult to trap otherwise. We then concentrate, transport, and release molecular or particulate payloads by precisely positioning and maneuvering the host droplets (Figure 5b–d, Movie S12, Supporting Information).

Inspired by living cells that regulate biochemical and metabolic processes by organizing biomolecules into temporary condensates,[26] we seek to employ the optothermal liquids as spatiotemporally controllable microreactors. In an exemplary experiment, we select a classical, cascade enzymatic reaction that produces fluorescent resorufin (Figure 5e; Note S7, Supporting Information) and switch from Sys. 1 to non-fluorescent Sys. 2. The droplet serves as a microreactor, as expected, to confine and enhance the reaction due to colocalization of the two sequential enzymes (Figure 5f; Movie S13, Supporting Information). We further highlight the on-demand, spatiotemporal addressability of the optothermal microreactors

by independently controlling their position, size, and on/off states (Figure 5g).

3. Conclusion

We have developed a laser-based, optothermal strategy to command phase separation with high addressability in space and time and have further showcased its capacity in liquid painting and liquid animation with high fidelity. Looking forward, we anticipate its implications in the fields of microfabrication, microelectronics, nonequilibrium physics, and cellular biology. For example, the liquid painting can be solidified by introducing cross-linkable monomers to generate permanent structures, complementary to the current, direct laser-writing technology.[27] The liquid patterns with concentrated electrolytes can act as reconfigurable conducting wires toward liquid circuits.[28] As an inherently out-of-equilibrium system, the continuous energy input by laser irradiation can drive convections inside and outside of the droplets, potentially directing fluid flow on a larger scale.[29] This optothermal strategy could be implemented in living cells with subcellular precision by engineering the cells to express thermal sensitive proteins and incubating them on an Au-coated substrate.[30]

Supporting Information

Supporting Information is available from the Wiley Online Library or from the author.

Acknowledgements

L.J. acknowledges support by National Natural Science Foundation of China (No. 22122201 and No. 21773092), Guangdong Natural Science Funds for Distinguished Young Scholar (No. 2018B030306011), and the Recruitment Program of Guangdong (No. 2016ZT06C322). Y.L. acknowledges support by National Natural Science Foundation of China (No. 61905092) and Guangdong Natural Science Funds for Distinguished Young Scholar (No. 2021B1515020046). M.T. acknowledges support by National Natural Science Foundation of China (No. 31971270).

Conflict of Interest

The authors declare no conflict of interest.

Author Contributions

X.C., T.W., and D.H. contributed equally to this work. X.C., T.W., D.H, Y.L, and L.J. conceived the experiments. Y.L. and L.J. oversee the entire project. Y.Z. and B.L. provided the experimental facilities. X.C. and T.W. constructed the optical setup and conducted optical experiments. D.H. explored various LLPS systems and optimized the microreactor. J.Z. established a Flory–Huggins model to account for LLPS in a temperature gradient. F.Z. wrote codes to realize liquidated music visualizer. All the authors analyzed the data and contributed to discussing the results and writing the paper.

Data Availability Statement

The data that support the findings of this study are available from the corresponding author upon reasonable request.

Keywords

coacervation, focused lasers, optothermal strategies, phase separation, programmable liquids

Received: June 19, 2022
Revised: July 24, 2022
Published online: August 21, 2022

[1] H. Ko, A. Javey, *Acc. Chem. Res.* **2017**, *50*, 691.
[2] W. Wang, J. V. I. Timonen, A. Carlson, D.-M. Drotlef, C. T. Zhang, S. Kolle, A. Grinthal, T.-S. Wong, B. Hatton, S. H. Kang, S. Kennedy, J. Chi, R. T. Blough, M. Sitti, L. Mahadevan, J. Aizenberg, *Nature* **2018**, *559*, 77.
[3] J. Forth, X. Liu, J. Hasnain, A. Toor, K. Miszta, S. Shi, P. L. Geissler, T. Emrick, B. A. Helms, T. P. Russell, *Adv. Mater.* **2018**, *30*, 1707603.
[4] E. Ahmed, D. P. Karothu, P. E. Naumov, *Angew. Chem., Int. Ed.* **2018**, *57*, 8837.
[5] T. H. Ware, M. E. McConney, J. J. Wie, V. P. Tondiglia, T. J. White, *Science* **2015**, *347*, 982.
[6] X. Zhang, C. L. Pint, M. H. Lee, B. E. Schubert, A. Jamshidi, K. Takei, H. Ko, A. Gillies, R. Bardhan, J. J. Urban, M. Wu, R. Fearing, A. Javey, *Nano Lett.* **2011**, *11*, 3239.
[7] A. A. Hyman, C. A. Weber, F. Jülicher, *Annu. Rev. Cell Dev. Biol.* **2014**, *30*, 39.
[8] F. Walton, K. Wynne, *Nat. Chem.* **2018**, *10*, 506.
[9] Y. Shin, J. Berry, N. Pannucci, M. P. Haataja, J. E. Toettcher, C. P. Brangwynne, *Cell* **2017**, *168*, 159.
[10] C. P. Brangwynne, C. R. Eckmann, D. S. Courson, A. Rybarska, C. Hoege, J. B. Gharakhani, F. Jülicher, A. A. Hyman, *Science* **2009**, *324*, 1729.
[11] L. Tian, N. Martin, P. G. Bassindale, A. J. Patil, M. Li, A. Barnes, B. W. Drinkwater, S. Mann, *Nat. Commun.* **2016**, *7*, 13068.
[12] Y. Yin, L. Niu, X. Zhu, M. Zhao, Z. Zhang, S. Mann, D. Liang, *Nat. Commun.* **2016**, *7*, 10658.
[13] D. Bracha, M. T. Walls, M.-T. Wei, L. Zhu, M. Kurian, J. L. Avalos, J. E. Toettcher, C. P. Brangwynne, *Cell* **2018**, *175*, 1467.
[14] X. Wang, P. Zhang, L. Tian, *Curr. Opin. Colloid Interface Sci.* **2021**, *52*, 101420.
[15] H. Yoo, C. Triandafillou, D. A. Drummond, *J. Biol. Chem.* **2019**, *294*, 7151.
[16] F. G..A. Quiroz, A. Chilkoti, *Nat. Mater.* **2015**, *14*, 1164.
[17] M. Orlishausen, W. Köhler, *J. Phys. Chem. B* **2015**, *119*, 8217.
[18] J. Berry, S. C. Weber, N. Vaidya, M. Haataja, C. P. Brangwynne, *Proc. Natl. Acad. Sci. USA* **2015**, *112*, 5237.
[19] A. D. Ward, M. G. Berry, C. D. Mellor, C. D. Bain, *Chem. Commun.* **2006**, *43*, 4515.
[20] D. T. Wasan, A. D. Nikolov, H. Brenner, *Science* **2001**, *291*, 605.
[21] D. G. Grier, *Nature* **2003**, *424*, 810.
[22] T. D. Ross, H. J. Lee, Z. Qu, R. A. Banks, R. Phillips, M. Thomson, *Nature* **2019**, *572*, 224.
[23] L. Lin, M. Wang, X. Peng, E. N. Lissek, Z. Mao, L. Scarabelli, E. Adkins, S. Coskun, H. E. Unalan, B. A. Korgel, L. M. Liz-Marzán, E.-L. Florin, Y. Zheng, *Nat. Photonics* **2018**, *12*, 195.
[24] X. Shan, F. Wang, D. Wang, S. Wen, C. Chen, X. Di, P. Nie, J. Liao, Y. Liu, L. Ding, P. J. Reece, D. Jin, *Nat. Nanotechnol.* **2021**, *16*, 531.

[25] I. A. Klein, A. Boija, L. K. Afeyan, S. W. Hawken, M. Fan, A. Dall'agnese, O. Oksuz, J. E. Henninger, K. Shrinivas, B. R. Sabari, I. Sagi, V. E. Clark, J. M. Platt, M. Kar, P. M. Mccall, A. V. Zamudio, J. C. Manteiga, E. L. Coffey, C. H. Li, N. M. Hannett, Y. E. Guo, T.-M. Decker, T. I. Lee, T. Zhang, J.-K. Weng, D. J. Taatjes, A. Chakraborty, P. A. Sharp, Y. T. Chang, A. A. Hyman, et al., *Science* **2020**, *368*, 1386.
[26] S. U. Setru, B. Gouveia, R. Alfaro-Aco, J. W. Shaevitz, H. A. Stone, S. Petry, *Nat. Phys.* **2021**, *17*, 493.
[27] C. A. Spiegel, M. Hippler, A. Münchinger, M. Bastmeyer, C. Barner-Kowollik, M. Wegener, E. Blasco, *Adv. Funct. Mater.* **2020**, *30*, 1907615.
[28] Z. Yang, Q. Zhuang, Y. Yan, G. Ahumada, B. A. Grzybowski, *J. Am. Chem. Soc.* **2021**, *143*, 16908.
[29] M. U. Mittasch, P. Gross, M. Nestler, A. W. Fritsch, C. Iserman, M. Kar, M. Munder, A. Voigt, S. Alberti, S. W. Grill, M. Kreysing, *Nat. Cell Biol.* **2018**, *20*, 344.
[30] J. A. Riback, C. D. Katanski, J. L. Kear-Scott, E. V. Pilipenko, A. E. Rojek, T. R. Sosnick, D. A. Drummond, *Cell* **2017**, *168*, 1028.